Shock Waves (2002) 12: 181–195
Digital Object Identifier (DOI) 10.1007/s00193-002-0163-0

Shock Waves

Investigations into water mitigation using a meshless particle method

M.B. Liu[1], G.R. Liu[1], K.Y. Lam[2]

[1] Center for Advanced Computations in Engineering Science, Department of Mechanical Engineering, National University of Singapore, 10 Kent Ridge Crescent, 119260 Singapore, Singapore
[2] Institute of High Performance Computing, 1 Science Park Road, 01-01 The Capricorn, 117528 Singapore, Singapore

Received 4 September 2001 / Accepted 19 February 2002
Published online 1 October 2002 –

Abstract. It is very difficult for traditional numerical methods to simulate the problems of water mitigation which has been increasingly used to reduce blast effects. This paper studies water mitigation problems by using smoothed particle hydrodynamics (SPH), which is a meshless, Lagrangian method appealing in treating large deformation explosion events with significant inhomogeneities. Numerical verifications considering high explosive detonation and underwater explosion shock waves have demonstrated the effectiveness of the SPH method, the solution procedure and the code. Contact and non-contact water mitigation simulations have been carried out and are compared with the case without mitigation. For either contact or non-contact water shield, the peak shock pressure and the equilibrium gas pressure are reduced to different levels according to the relevant geometry of the system setup. An optimum contact water shield thickness is found to produce the best mitigation effect for a given high explosive charge, while the non-contact water shield, if properly designed, can result in further reduction of the peak shock pressure and the equilibrium gas pressure.

Key words: Water mitigation, Smoothed particle hydrodynamics, Meshless method, Particle method, Detonation, Shock wave

1 Introduction

The detonation of high explosives produces extremely intense shock waves within a very short time. The blast effects caused by the detonation either in air or under water are of great significance to nearby persons and structures. Researchers from the defense and academic areas have been looking for ways to effectively mitigate blast effects and thus reduce the consequent damages. One of the comparatively new concepts is water mitigation, in which a shield of water is placed in the near proximity of explosives, not necessarily in contact, to change the generation and propagation of air blast waves (Fig. 1 illustrates water held in plastic bags as a bomb shelter to mitigate blast effects). A water shield can be used not only as an effective barricade that stops debris and splinters, but also as an excellent blast mitigator to reduce blast shock and internal equilibrium gas pressure in a confined space. Practically, water can be either held in plastic bags for short-term applications such as bomb disposal or held in plastic tanks for long-term applications, especially for those where accidental damage may happen.

Correspondence to: G.R. Liu
(e-mail: mpeliugr@nus.edu.sg)

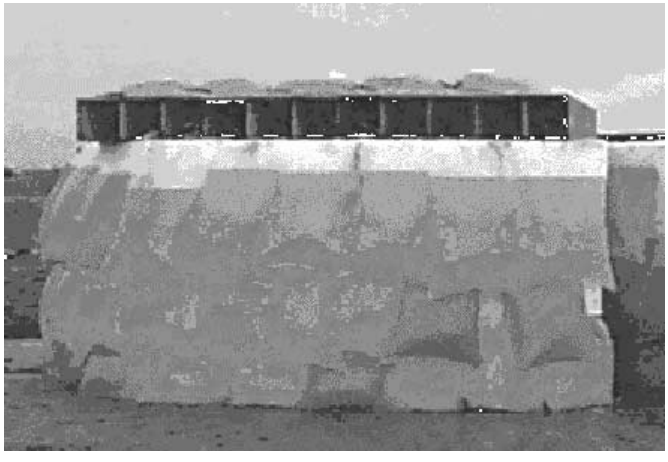

Fig. 1. An illustration of water mitigation: water held in plastic bags as a bomb shelter

Many feasibility tests for mitigation problems have been carried out. However, due to the intense interest in this field by the defense area, very few documents are publicly available. The NCEL tests (Keenan and Wager 1992) were conducted at the David Taylor Research Center for the Naval Civil Engineering Laboratory (NCEL).

In the tests, 4.67 lb. of TNT explosive were tested in a confined chamber, first without, and then surrounded by water. Both the equilibrium gas pressure and impulse were reduced by about 90%. In the USACE Huntsville tests (Marchand et al. 1996), water bags were added around unexploded ordnance in a container. The experimental results show that the equilibrium gas pressure was successfully reduced by approximately 70%. In the small-scale Alvdalen tests (Forsen et al. 1996), it has been also observed that putting water around explosives, either in contact or not, leads to pressure reduction. However, the large-scale Alvdalen tests (Forsen et al. 1997; Hansson and Forsen 1997) did not reveal any effects of water mitigation due to other variations in the experimental setup.

To develop an efficient water mitigation system, sufficient parametric studies are necessary. Numerical simulation provides an alternative greatly reducing the number of expensive and dangerous firing tests. However, the documents related to numerical simulations of water mitigation are also very limited, on the one hand, for the reason of confidentiality, and on the other hand, due to the numerical difficulties inherent in the water mitigation simulations. Challenges such as large deformations, large inhomogeneities, moving interfaces etc. confront investigators. Chong et al. (1998a,b, 1999) investigated the water mitigation effects on an explosion inside a vented tunnel system and ascertained the mitigation effects of water in reducing the maximum peak shock pressure. Shin et al. (1998) investigated a water mitigation problem in the quasi-one-dimensional spherical infinite computational domain by using the multi-material Eulerian finite element technique of the software MSC/Dytran. Their numerical results show that the peak shock pressure generally decreases and the shock arrival time increases. Zhao studied water mitigation effects on detonation in a confined chamber (Zhao et al. 1998) as well as the water effects on shock wave delay in the free field (Zhao 2001). It is reported that the peak shock pressure is reduced by about 17-46% when explosives are surrounded by water with an amount of 1-5 times the explosive mass. Some other references (Crepeau and Needham 1998; Malvar and Tancreto 1998) also contain numerical simulations and comparisons with experimental data. The emerged literature usually applies some kind of hydrocode, which generally uses model discretizations that are fixed in space, but allows for mass, momentum and energy transfer across cells.

This paper studies water mitigation problems by using smoothed particle hydrodynamics (SPH). SPH was originally invented for solving astrophysical problems in three-dimensional open space (Lucy 1977; Gingold and Monaghan 1977), and later extended to other areas, especially those with large deformations and inhomogeneities (Swegle and Attaway 1994; Randles and Libersky 1996; Liu et al. 2000, 2001, 2002). In the SPH method, smoothed particles are used as interpolation points to represent materials at discrete locations, so it is possible to obtain the history of the fluid particles in a natural way, and thus easily trace material interfaces, free surfaces and moving boundaries. The meshless nature of the SPH methodology overcomes the difficulties related to large deformations, since SPH uses particles or points rather than a mesh as the computational frame to interpolate. These nice features of SPH make it fairly attractive in simulating water mitigation problems and the related physics.

The objective of this paper is to investigate water mitigation phenomena as well as the relationship of water mitigation effects and setup geometries. To verify the SPH method, the numerical procedure and the code, the results are compared with the theoretical values and/or experimental data for a one-dimensional TNT slab detonation problem and an underwater explosion problem with a spherical charge. Water mitigation simulations are carried out for a square-shaped TNT charge detonating in a confined square chamber with different setups of water shields and/or air gaps.

2 Water mitigation and governing equations

Water mitigation is a complex non-linear wave propagation phenomenon, rather than an ordinary underwater explosion problem or an acoustic water-air interface problem. It involves the high explosive (HE) detonation and interaction of the explosive gas, water shield and outside air. The detonation-produced blast waves propagate outward in all directions and aerosolize the surrounding water shield. On the one hand, since the density of water is much higher than that of air, when the particles of the explosive gases strike the water particles, they are suddenly slowed down due to momentum exchange with the water particles. The water jacket delays the arrival of the shock wave and reduces the magnitude of the peak shock pressure. On the other hand, the aerosolized water expanding with the explosive gas absorbs the detonation energy of the explosive, and thus reduces the peak shock pressure, and, in the case of detonation in a rigidly confined chamber, reduces the equilibrium gas pressure.

Due to the extremely high detonation and expansion speed, the explosive gas, water shield and outside air can be assumed to be inviscid, while the whole water mitigation process is adiabatic. So, the Euler equations coupled with a suitable equation of state can be used to model the water mitigation process:

$$\begin{cases} \dfrac{D\rho}{Dt} = -\rho \nabla \cdot \boldsymbol{v} \\ \dfrac{D\boldsymbol{v}}{Dt} = -\dfrac{1}{\rho}\nabla p \\ \dfrac{Du}{Dt} = -\dfrac{p}{\rho}\nabla \cdot \boldsymbol{v} \\ p = p(\rho, u) \end{cases}, \tag{1}$$

where ρ, u, p, $\boldsymbol{v}$ and t are density, specific internal energy per unit mass, pressure, velocity vector and time, respectively. The first three equations in (1) represent the conservation of mass, momentum, and energy, while the fourth equation is the equation of state (EOS).

Table 1. Material parameters and coefficients in the EOS for TNT

Symbol	Meaning	Value
ρ_0	Initial density	1630 kg/m^3
D	Detonation velocity	6930 m/s
P_{CJ}	CJ pressure	21 GPa
A	Fitting coefficient	371.2 GPa
B	Fitting coefficient	3.21 GPa
R_1	Fitting coefficient	4.15
R_2	Fitting coefficient	0.95
ω	Fitting coefficient	0.30
E_0	Detonation energy	4.29 MJ/kg

3 Equation of state

The pressure-volume-energy behavior or equations of state for the explosive (TNT), water and air are important for the simulation. For the detonation-produced explosive gas, the standard Jones-Wilkins-Lee (Dobratz 1981), or JWL, equation of state is employed, which corresponds to a detonation velocity of 6930 m/s and a Chapman-Jouguet (CJ) pressure of 21 GPa. The pressure of the explosive gas is:

$$p = A\Big(1-\frac{\omega\eta}{R_1}\Big)e^{-R_1/\eta}+B\Big(1-\frac{\omega\eta}{R_2}\Big)e^{-R_2/\eta}+\omega\eta\rho_0 E\ , \quad (2)$$

where η is the ratio of the density of detonation products to the initial density of the original explosive; E is the specific internal energy per unit mass; A, B, R_1, R_2, ω are fitting coefficients. The values of the corresponding coefficients are listed in Table 1.

Air is modeled as an ideal gas, which satisfies the gamma-law equation of state:

$$p = (\gamma - 1)\rho E\ , \quad (3)$$

where γ is the ratio of specific heats and is taken as 1.4; E is the specific internal energy per unit mass. In the simulation, the initial density of air is taken as 1 kg/m^3; therefore the initial energy of air is $2.5 \cdot 10^5$ J/kg, which corresponds to the pressure of 1 bar according to Eq. (3).

The pressure-volume-energy behavior of water has been widely studied under different shock loadings of high pressures, densities and temperatures. Water can be modeled as a compressible fluid with the Mie-Grüneisen equation of state, which uses a cubic shock velocity and fluid particle velocity to determine the pressure of compressed and expanded water. Shock Hugoniot experimental data are needed to correlate the cubic shock-velocity/particle-velocity equation:

$$\frac{U_s - C_0}{U_s} = S_1\left(\frac{U_s}{U_p}\right) + S_2\left(\frac{U_s}{U_p}\right)^2 + S_3\left(\frac{U_s}{U_p}\right)^3\ , \quad (4)$$

where U_s, U_p, and C_0 are the shock wave velocity, fluid particle velocity and initial sound speed, respectively; S_1, S_2, and S_3 are the coefficients to determine the slope of the U_s-U_p curve.

Table 2. Material parameters and coefficients in the EOS for water

Symbol	Meaning	Value
ρ_0	Initial density	1000 kg/m^3
C	Sound speed	1480 m/s
γ_0	Grüneisen coefficient	0.5
a	Volume correction coefficient	0
S_1	Fitting coefficient	2.56
S_2	Fitting coefficient	1.986
S_3	Fitting coefficient	1.2268

Shin et al. (1998) provided a comparison of several approximations to shock Hugoniot experimental data due to uncertainties in the data for water. In this simulation, the Steinberg (1987) experimental data is used.

The pressure of water under compression is given by:

$$p = \frac{\rho_0 C^2\mu\left[1+\left(1-\frac{\gamma_0}{2}\right)\mu-\frac{a}{2}\mu^2\right]}{\left[1-(S_1-1)\mu-S_2\frac{\mu^2}{\mu+1}-S_3\frac{\mu^3}{(\mu+1)^2}\right]^2}+ +(\gamma_0+a\mu)E\ . \quad (5)$$

In the case of expansion, the pressure of water is

$$p = \rho_0 C_0^2\mu + (\gamma_0 + a\mu)E\ , \quad (6)$$

where ρ_0 is the initial density; η is again the ratio of the densities after and before disturbance; E is the specific internal energy per unit volume and thus possesses the same unit of Pa as pressure does; $\mu = \eta - 1$ ($\mu > 0$ for compressed state, $\mu < 0$ for expanded state). Some material parameters and coefficients in the EOS for water are listed in Table 2.

Chisum and Shin (1997) provided a procedure to convert the above Grüneisen equation of state for water into polynomial form either for a compressed or expanded state. Under compression, we have:

$$p = a_1\mu + a_2\mu^2 + a_3\mu^3 + (b_0 + b_1\mu + b_1\mu^2)\rho_0 E\ , \quad (7)$$

while under expansion:

$$p = a_1\mu + (b_0 + b_1\mu)\rho_0 E\ . \quad (8)$$

The constants in Eqs. (7) and (8) were determined, for both compression and expansion states, by matching terms in Eqs. (3) and (6) with the Steinberg (1987) shock Hugoniot data. Hence, the above equation of state for water can be used over the range where the Mie-Grüneisen EOS is valid. It is to be noted that in contrast to Eqs. (3) and (6), E in Eqs. (7) and (8) is the specific internal energy per unit mass. The constants for condensation values on the order of $\mu < 0.8$ are as follows: $a_1 = 2.19$ GPa, $a_2 = 9.224$ GPa, $a_3 = 8.767$ GPa, $b_0 = 0.4934$, $b_1 = 1.3937$.

4 The SPH method and related numerical aspects

The SPH method has been extensively studied and widely applied in the last decades. The combination of meshless and Lagrangian nature inherent in the SPH method makes it very attractive in treating large deformations, large inhomogeneities and moving boundaries in extremely transient detonation events.

4.1 Basics of SPH

In the SPH method, the fluid is represented by particles, which are typically of fixed mass, follow the fluid motion, advect contact discontinuities, and reduce computational diffusion of various fluid properties. The particles carry fluid quantities such as mass m, velocity vector $\boldsymbol{v}$, position vector $\boldsymbol{x}$ etc. and form the computational frame for the partial differential equations representing the conservation laws. In the standard SPH method, for a function f, the approximation of its value at a certain location or particle i as well as its gradient can be expressed as summation interpolants over the neighboring particles using a smoothing kernel function W with the smoothing length h:

$$\langle f_i \rangle = \sum_{j=1}^{N} \left(\frac{m_j}{\rho_j} \right) f_j W_{ij} \ ; \tag{9}$$

$$\langle \nabla f_i \rangle = \sum_{j=1}^{N} \left(\frac{m_j}{\rho_j} \right) f_j \nabla_i W_{ij} \ , \tag{10}$$

where, denoting the distance between particles i and j as r_{ij},

$$W_{ij} = W(\boldsymbol{x}_i - \boldsymbol{x}_j, h) = W(|\boldsymbol{x}_i - \boldsymbol{x}_j|, h) \ , \tag{11}$$

$$\nabla_i W_{ij} = \frac{\boldsymbol{x}_i - \boldsymbol{x}_j}{r_{ij}} \frac{\partial W_{ij}}{\partial r_{ij}} = \frac{\boldsymbol{x}_{ij}}{r_{ij}} \frac{\partial W_{ij}}{\partial r_{ij}} \ . \tag{12}$$

A typical smoothing kernel function should satisfy the normalization condition $\int W(\boldsymbol{x} - \boldsymbol{x}', h) \mathrm{d}\boldsymbol{x} = 1$, the Delta function condition $\lim_{h \to 0} W(\boldsymbol{x} - \boldsymbol{x}', h) = \delta(\boldsymbol{x} - \boldsymbol{x}')$, and the compactness condition $W(\boldsymbol{x} - \boldsymbol{x}', h) = 0$ for $|\boldsymbol{x} - \boldsymbol{x}'| > \lambda h$, where λ is a constant dependent only on the particular smoothing kernel function. In this paper, a cubic spline function is used (Monaghan 1992):

$$W(S,h) = \alpha_d \times \begin{cases} \frac{2}{3} - S^2 + \frac{1}{2} S^3 & \text{for } 0 < S \leq 1; \\ \frac{1}{6}(2-S)^3 & \text{for } 1 < S \leq 2; \\ 0 & \text{for } S > 2, \end{cases} \tag{13}$$

where $S = |\boldsymbol{x} - \boldsymbol{x}'|/h$, α_d is a dimension-dependent constant related to the smoothing length. In one, two or three-dimensional space, $\alpha_d = 1/h$, $15/7\pi h^2$ or $3/2\pi h^3$, respectively. It is clear that λ used in this cubic spline kernel is equal to 2.

4.2 Artificial viscosity

Artificial viscosity is used in the SPH methodology to stabilize the numerical scheme, prevent particle penetration and capture shock waves. In this paper, we employ the standard artificial viscosity Π_{ij} (Monaghan 1992):

$$\Pi_{ij} = \begin{cases} \dfrac{-\alpha_\Pi \bar{c}_{ij} \phi_{ij} + \beta_\Pi \phi_{ij}^2}{\bar{\rho}_{ij}} & \text{for } \boldsymbol{v}_{ij} \cdot \boldsymbol{x}_{ij} < 0; \\ 0 & \text{for } \boldsymbol{v}_{ij} \cdot \boldsymbol{x}_{ij} \geq 0, \end{cases} \tag{14}$$

$$\phi_{ij} = \frac{h_{ij} \boldsymbol{v}_{ij} \cdot \boldsymbol{x}_{ij}}{|\boldsymbol{x}_{ij}|^2 + \varphi^2}, \quad \boldsymbol{v}_{ij} = \boldsymbol{v}_i - \boldsymbol{v}_j, \tag{15}$$

$$h_{ij} = \frac{1}{2}(h_i + h_j) \ , \quad c_{ij} = \frac{1}{2}(c_i + c_j) \ , \quad \rho_{ij} = \frac{1}{2}(\rho_i + \rho_j) \ , \tag{16}$$

where α_Π, β_Π, φ are constants that are set to 1, 1 and $0.1 h_{ij}$, respectively; $\boldsymbol{v}$ and c represent the velocity vector and the speed of sound.

4.3 Equation of motion

Coupling with the equations of state, the following equation of motion is derived as one of the standard form of SPH equations which can be used to model water mitigations:

$$\begin{cases} \dfrac{D\rho_i}{Dt} = \displaystyle\sum_{j=1}^{N} m_j (\boldsymbol{v}_i - \boldsymbol{v}_j) \cdot \nabla_i W_{ij} \\ \dfrac{D\boldsymbol{v}_i}{Dt} = -\displaystyle\sum_{j=1}^{N} m_j \left(\frac{p_i}{\rho_i^2} + \frac{p_j}{\rho_j^2} + \Pi_{ij} \right) \nabla_i W_{ij} \\ \dfrac{Du_i}{Dt} = \dfrac{1}{2} \displaystyle\sum_{j=1}^{N} m_j \left(\frac{p_i}{\rho_i^2} + \frac{p_j}{\rho_j^2} + \Pi_{ij} \right) (\boldsymbol{v}_i - \boldsymbol{v}_j) \cdot \nabla_i W_{ij} \\ \dfrac{D\boldsymbol{x}_i}{Dt} = \boldsymbol{v}_i \end{cases} \tag{17}$$

Using some standard techniques such as the leapfrog (LF), predictor-corrector and Runge-Kutta (RK) schemes it is possible to carry out the numerical integration of ordinary differential equations for physical variables at every particle. In this paper, the leapfrog method is used because of its low memory requirements and good efficiency. The particle density, velocity, internal energy and position can be updated according to the following:

$$\begin{cases} \rho_i(t + \Delta t/2) = \rho_i(t - \Delta t/2) + \Delta t \cdot D\rho_i(t) \\ \boldsymbol{v}_i(t + \Delta t/2) = \boldsymbol{v}_i(t - \Delta t/2) + \Delta t \cdot D\boldsymbol{v}_i(t) \\ u_i(t + \Delta t/2) = u_i(t - \Delta t/2) + \Delta t \cdot Du_i(t) \\ \boldsymbol{x}_i(t + \Delta t) = \boldsymbol{x}_i(t) + \Delta t \cdot \boldsymbol{v}_i(t + \Delta t/2) \end{cases} \tag{18}$$

However, the LF is subjected to the Courant-Friedrichs-Lewy (CFL) stability condition, which typically results in the time step proportional to the smoothing length. In this work, the time step is taken as

$$\Delta t = \min \left(\xi h_i / [h_i \nabla \cdot \boldsymbol{v}_i + c_i + 1.2(\alpha_\Pi c_i + \beta_\Pi |\nabla \cdot \boldsymbol{v}_i|)] \right), \tag{19}$$

where ξ is the Courant number taken as ~ 0.3.

4.4 Smoothing length evolution

The smoothing length h is very important in SPH, since it directly influences the efficiency and accuracy. If h is taken too small, there may be not enough particles in the designated range of λh to exert forces on the particle, which results in low accuracy. If the smoothing length is too large, all details of the particle or local properties may be smoothed out, and the accuracy would be low as well. In water mitigation simulations, large density inhomogeneities exist. This work adapts the smoothing length in such a manner that only a minimum necessary number of neighboring particles contribute to the discrete summations.

Let us suppose that h_i^0 is the initial smoothing length of particle i, while N_i^0 is the number of the initial neighboring particles within the smoothing range λh_i^0 for particle i. For example, in one, two or three-dimensional space N_i^0 may be taken as 5, 21 and 57, respectively. This N_i^0 corresponds to the number of neighboring particles on a cubic lattice with a smoothing length slightly bigger than the particle spacing, e.g. 1.2 times the particle spacing, and the cubic spline-smoothing kernel that extends to $2h$. The particle has mass m_i and remains unchanged during the computation. Then the initial smoothing length h_i^0 can be calculated based upon the initial density of the particle:

$$h_i^0 = c_d \times \left(\frac{\sum_{j=1}^{N_i^0} m_j}{\rho_i^0} \right)^{1/d} , \qquad (20)$$

where c_d is a dimension-dependent coefficient. For one, two and three-dimensional space ($d = 1, 2, 3$) it equals to $1/4$, $(1/4\pi)^{1/2}$ and $(3/32\pi)^{1/3}$, respectively.

The smoothing length of each particle can be updated by the following most commonly used expression:

$$\frac{Dh_i^n}{Dt} = -\frac{h_i^n}{\rho_i^n d} \sum_{j=1}^{N} m_j (\boldsymbol{v}_i^n - \boldsymbol{v}_j^n) \cdot \nabla_i^n W_{ij} , \qquad (21)$$

where h_i^n, ρ_i^n, $\boldsymbol{v}_i^n$, $\nabla_i^n W_{ij}$ are the smoothing length, density, velocity, and kernel gradient of particle i at time step n.

Equation (21) is generally used to update the smoothing length: $h_i^{n+1} = h_i^n + \mathrm{d}h_i^n/\mathrm{d}t$. It works well in homogenous, slowly expanding or contracting gases. However, for problems with high deformations, or problems with large density inhomogeneities, it may not be very accurate and stable. In order to model water mitigation problems with large density inhomogeneities, a procedure for the smoothing length optimization is employed to update h_i^{n+1} so that each particle interacts with roughly a constant number of neighboring particles. This procedure consists of two steps: the prediction step and the correction step.

Prediction step: Update h_i^{n+1} as $h_i^{n+1} = h_i^n + \theta \times \mathrm{d}h_i^n/\mathrm{d}t$, where θ is a relaxation factor taken as 1.0 at first and then adjusted slightly around 1.0 in the subsequent optimization and relaxation step.

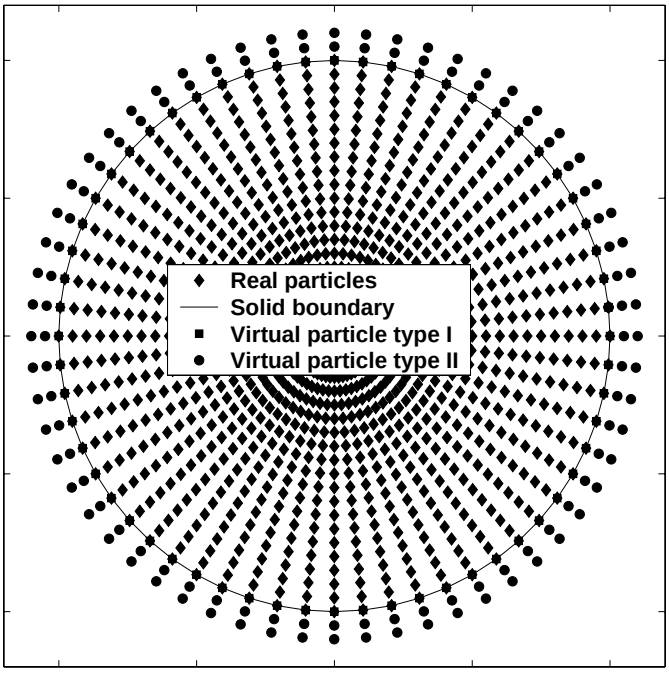

Fig. 2. Illustration of real particles and the two types of virtual particles as well as the solid boundary

Correction step: Once h_i^{n+1} is obtained, the current number of neighbors N_i^{n+1} can be then determined. If N_i^{n+1} is found to be roughly the same as N_i^0, it is desirable situation. If it is different from N_i^0 by more than a small, prescribed tolerance of few percent (in this paper, 5%), then the relaxation factor θ should be adjusted around 1.0 to get a new h_i^{n+1} until N_i^{n+1} is roughly the same as N_i^0.

4.5 Solid boundary condition

In our work, two types of virtual particles are used to treat the solid boundary condition (Fig. 2). The particles of the first type are located right on the solid boundary and are similar to what was used by Monaghan (1994). The virtual particles of the second type fill in the exterior, near-boundary region and are similar to what was used by Libersky and Petsheck (1993). The virtual particles of the second type are constructed in the following way. For a certain real particle i within the smoothing area λh_i inside the computational domain, a virtual particle is placed symmetrically outside of the domain. These virtual particles have the same density and pressure as the corresponding real particles but opposite velocities. These virtual particles are not enough to prevent the real particles from penetrating the boundary. This leads to the application of the virtual particles of the first type, which are used to produce a sufficient repulsive boundary force, when a particle approaches the boundary. Thus, for a boundary particle i, all the neighboring particles $N(i)$ within its influencing area of λh_i can be categorized into three subsets:

- $I(i)$: all the interior particles that are the neighbors of i (real particles);

– $B(i)$: all the boundary particles that are the neighbors of i (virtual particles of type I);
– $E(i)$: all the exterior particles that are the neighbors of i (virtual particles of type II).

The two types of virtual particles are specially marked for contribution in the subsequent summation on the real particles. The virtual particles of the first type not only take part in the kernel and the particle approximation for the real particles, but also exert a repulsive penalty force on the particles approaching the solid boundary. The position and physical variables of these virtual particles, however, do not evolve in the simulation process. A repulsive force similar to the Lennard-Jones molecular force is applied pairwisely between the first type virtual particles and the approaching real particles along the line connecting the centers of the two interacting particles (Monaghan 1994). The repulsive force prevents the interior real particles from penetrating the solid boundary nonphysically.

The virtual particles of the second type do not evolve their parameters; at the next time step another set of them is produced in the same way. Our numerical tests have shown that this treatment of the boundary is very stable and effective. It not only improves the accuracy of the SPH approximation in the boundary region, but also prevents the unphysical particle penetration across the solid boundary.

5 Numerical verifications

Since water mitigation involves an interaction of high explosive, water and air, two numerical examples are presented to verify the effectiveness of the SPH method and the code in treating high explosive detonation and underwater explosion shocks. The first benchmark is a one-dimensional TNT slab detonation (Liu et al. 2001), in which a 0.1 m long TNT slab initiates from one end to another. Figure 3 shows the pressure profiles along the slab at 1 μs intervals from 1 to 14 μs, when the solid boundary condition is applied to the end of initiation. The presented results are in close agreement with those from an Eulerian method (Shin and Chisum 1997). It can be seen that, with the process of detonation, the detonation pressure converges to the experimentally determined C-J pressure. The magnitude, location and profile of the detonation wave are well predicted. The gas behind the detonation wave front has a pressure profile similar to exponential decay, with the peak shock pressure immediately behind the detonation wave front and the decay length increasing with propagation distance. If the free boundary condition is applied to the end of initiation, the advancement of the detonation wave through the explosive is accompanied by the rarefaction wave propagation from outside. The expansion of the gaseous products results in lower pressure, density and velocity as compared with the case of the solid wall boundary, where no rarefaction wave propagates inward to the gas. Figure 4 shows the detonation wave and the pressure profiles at 1 and 2 μs. The solid lines represent the analytical solution (Zhang 1976),

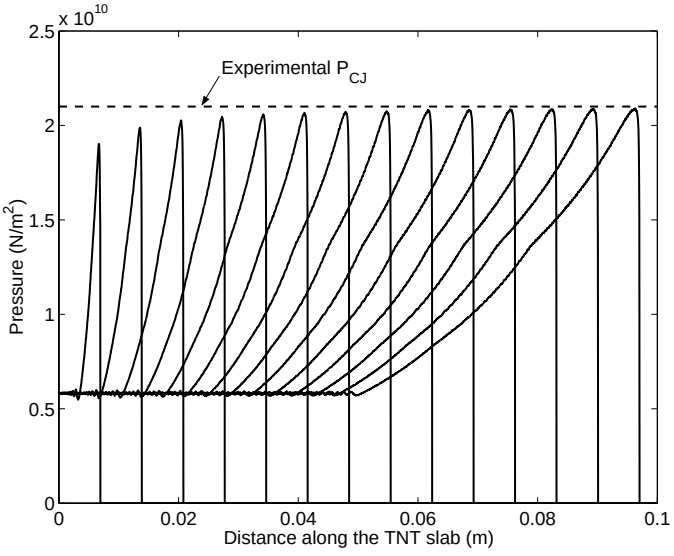

Fig. 3. Pressure profiles along the TNT slab during the detonation process for the solid wall boundary condition

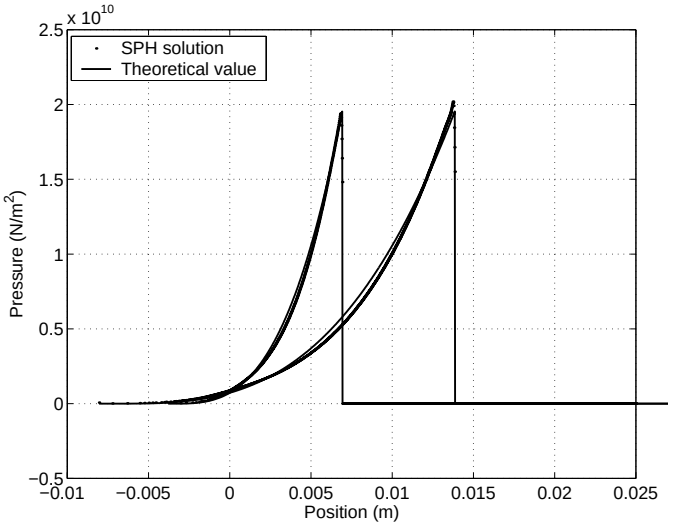

Fig. 4. The detonation wave and the pressure profiles at 1 and 2 μs for the free boundary condition

while the dots represent the SPH simulation results. The pressure distributions obtained by the SPH method nearly coincide with those from the analytical solution.

The second numerical verification is an underwater explosion shock problem. Underwater explosion consists of the detonation process of the original high explosive, the expansion process of the explosive gas into the surrounding water, and the interaction with nearby structures. As the detonation wave reaches the interface between the explosive and the surrounding water, a high-pressure shock wave with a blast profile is transmitted to propagate through the water. In the whole process of underwater explosions, some special features such as large deformations, large inhomogeneities, moving material interfaces, deformable boundaries, and free surfaces exist. In the simulation, a 137 kg spherical (with the charge radius of approximately 0.27 m) TNT charge explodes in

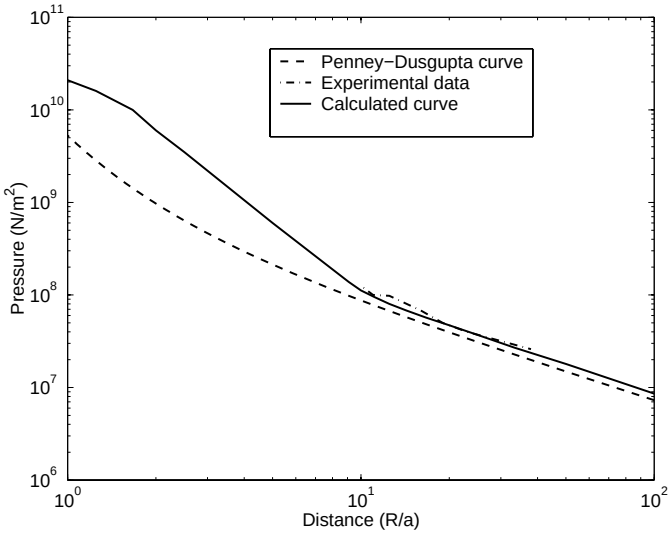

Fig. 5. Underwater peak pressures at different locations for a spherical TNT charge

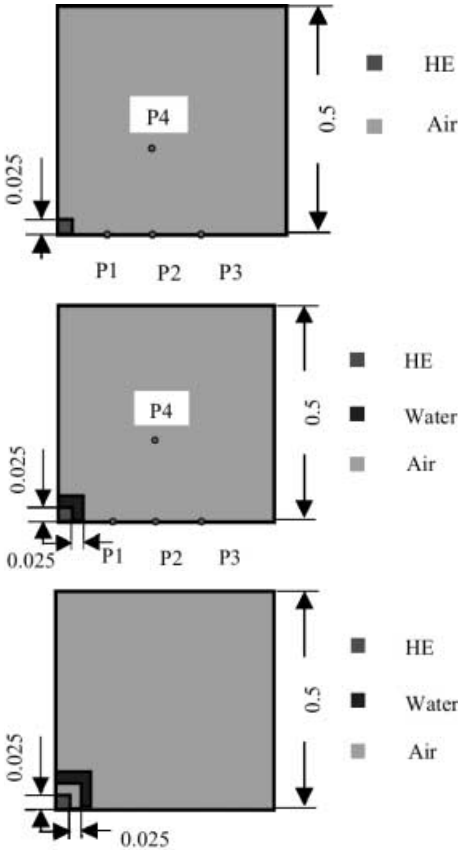

Fig. 6. Setups of the simulations

water. In this quasi-1D simulation, 2700 particles are deployed along the diameter with 1350 particles on either side from the charge center. Figure 5 shows the detailed comparisons of peak shock pressures with the experimental data (Cole 1948) and the Penney and Dusgupta (1942) theoretical values. In the logarithm-scaled figure, a is the radius of the original HE charge; R is the distance from the pressure measurement location to the charge center.

Table 3. Locations of the observation points

Point	Coordinate	Normalized distance
1	(0.0, 0.1)	4
2	(0.0, 0.2)	8
3	(0.0, 0.3)	12
4	(0.2, 0.2)	11.3

The theoretical values and the experimental data are only valid for the region of $R/a > 10$, where the calculated results agree well with them.

6 Simulation setups

In this paper we consider a square-shaped (0.05 m × 0.05 m) TNT charge which detonates and then expands outwards. Figure 6 shows one quarter of the initial geometry of the two-dimensional models. For this planarly symmetrical problem, $x = 0$ and $y = 0$ represent the planes of symmetry. Four observation points are chosen to measure pressure and shock wave arrival time. Taking the central point of the geometry as the origin, the locations of the four points as well as their distances to the central point, normalized by the explosive thickness (0.025 m) are listed in Table 3.

In the simulation, three different cases are comparatively modeled. The first case (Fig. 6a) is the explosive detonation in air without water mitigation; the second case (Fig. 6b) is the water mitigation with water and the explosive directly in contact; and the last one (Fig. 6c) is the non-contact water mitigation with an air gap between the explosive and the water shield. In the contact water mitigation, the water shield thickness is varied from 0.01 m to 0.045 m, which correspond to 0.4 to 1.8 times the explosive thickness. For the case of a non-contact water shield, the mitigation effects for a water shield thickness of 0.025 m and 0.05 m are investigated with the same air gap thickness of 0.025 m. For these three cases, the simulations are carried out for a rigidly confined chamber. Actually, free field water mitigations could be also investigated, even easier than the confined water mitigation, since the SPH method is more natural to treat moving free boundaries. However, in free field water mitigation, only the reducing effect on the peak shock pressure can be investigated. The final equilibrium gas pressure will, with the expansion of the volume, decrease as low as the ambient pressure. In confined water mitigation, both important parameters, the peak shock pressure and the equilibrium gas pressure, can be studied.

7 Simulation results

7.1 Explosion shock wave in air

An unmitigated explosion produces blast shock waves in air and throws out solids, such as debris from craters or

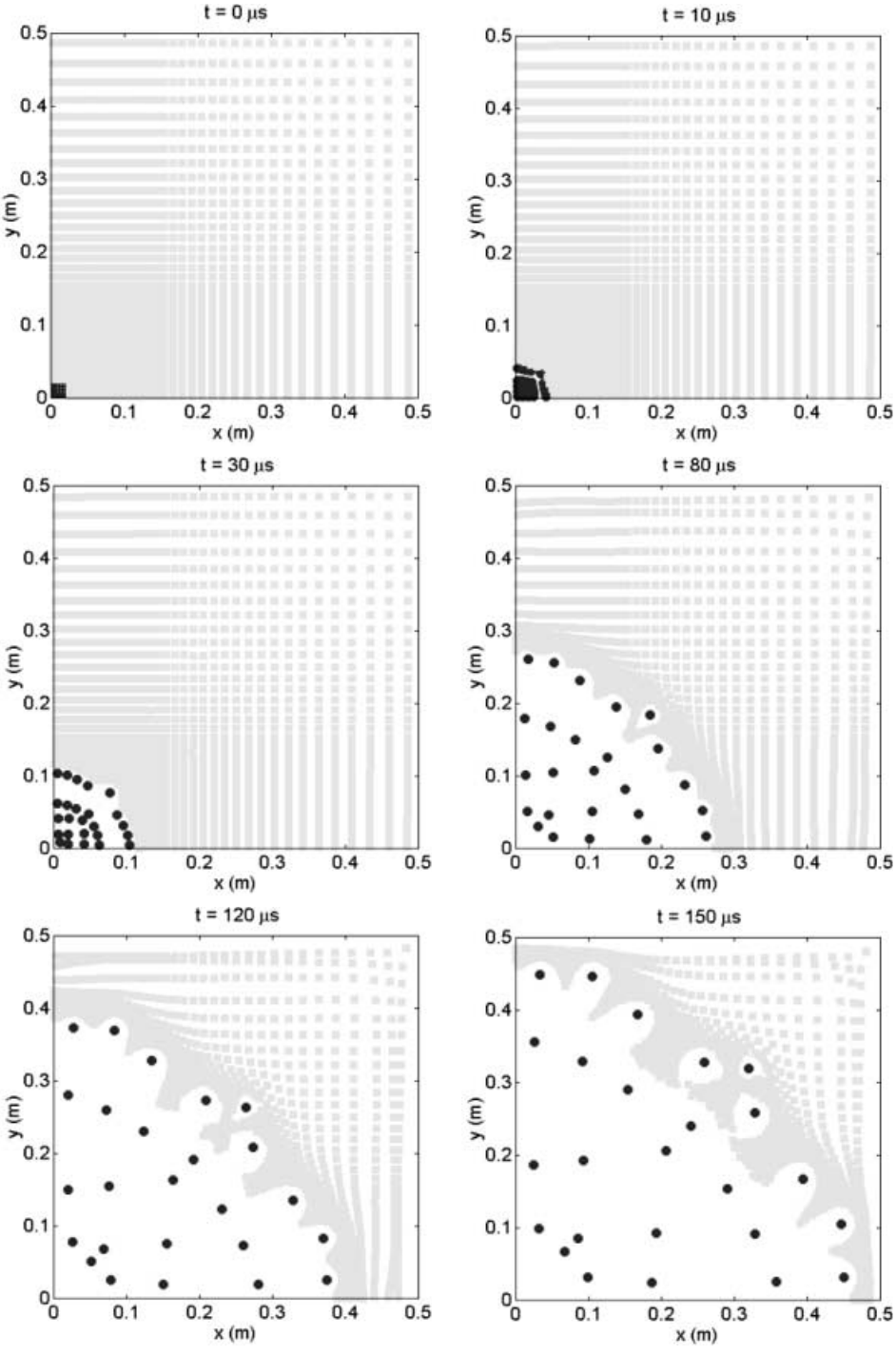

Fig. 7. Particle distributions in the explosion process in air

steel splinters from military shells and bombs. Inside a container, such as a building, it produces high gas pressure, which bursts the walls and makes its debris fly. After detonation of the explosive TNT, shock waves propagate outward with rarefaction waves advancing from outside to the inner gas. The peak shock pressure decay quickly with the propagation of the shock and the increasing volume of the explosive gas. Figure 7 shows the particle distribution in the explosion process at six representative instants. The small circles and squares represent explosive gas particles and air particles, respectively. The initial particles are exponentially distributed outwards so that to ensure that the number of gas particles is sufficient although the area occupied by them is much smaller than the entire computational domain. The original square-shaped explosive gas gradually turns into a circle. The air particles near the gas/air interface are highly compressed due to the impulsively driven pressure. At the same distance from the

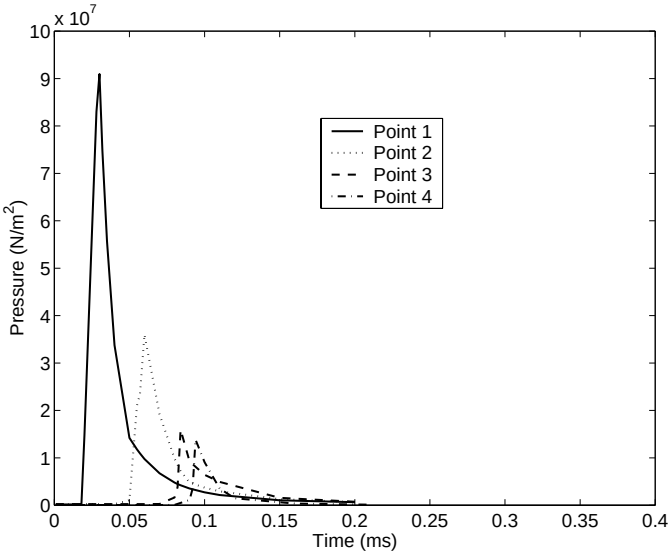

Fig. 8. Pressure histories at four observation points for the explosion process in air

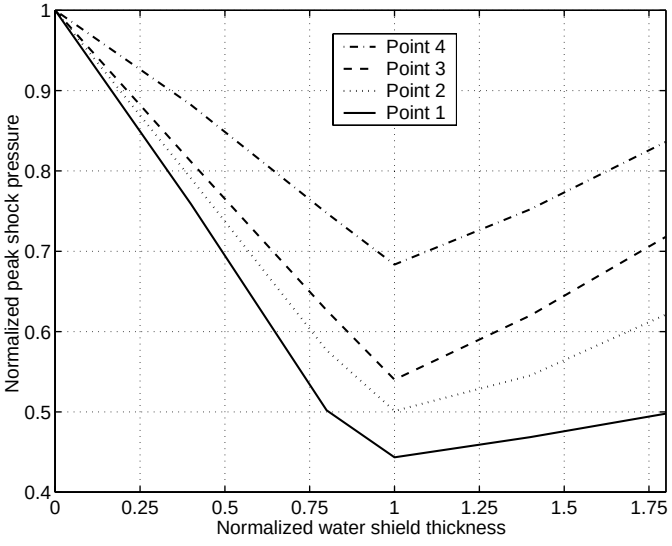

Fig. 9. Normalized peak shock pressures for different water shield thicknesses

origin, the particle velocities around the symmetric planes $x = 0$ and $y = 0$ are higher than those around the symmetric plane $x = y$, while the particle pressure around the symmetric planes $x = 0$ and $y = 0$ are lower than that around the symmetric plane $x = y$.

As seen from Fig. 7, some large circles are produced when the explosive gas particles drastically interact with the outside air particles. Further investigations show that increasing the number of particles does not eliminate the circles. It is suggested that this may be caused by the SPH method itself when simulating problems with very large inhomogeneities (density differences) in the drastically interacting process. In the SPH method, the particle mass remains unchanged, while particle density or volume evolves in the simulation. The density of the highly compressed explosive gas is much higher than that of the outside air (1630 times, since the density of air is 1 kg/m^3 while the

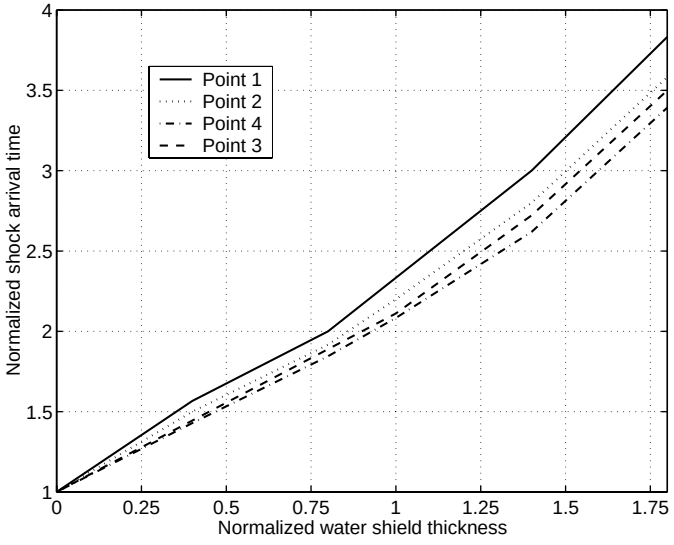

Fig. 10. Normalized shock arrival times for different water shield thicknesses

density of the initial explosive gas is 1630 kg/m^3). Around the interface of the explosive gas and air, the gas particles tend to occupy much more space than the original volume with the unchanged particle mass, and therefore cause the fragmentation-like large circles in Fig. 7. If the density difference is not so large, this fragmentation-like phenomena do not happen.

Figure 8 shows pressure histories for the four observation points. As expected, the calculated pressures at these four points initially stay around 1 bar, later suddenly rise to the peak values, and then quickly decay in an exponential way. With the propagation of the shock wave, the peak shock pressures decrease while the shock wave front becomes smoother. At further points, the shock arrives at later stages with slower decay rate since the pressures there are lowered while the particle volume is further expanded.

Since the chamber is rigidly confined, at very late stages the shock waves decay in the course of many forward and backward reflections from the rigid wall and interactions of the forward and backward shock waves. The mixture of the gas and air gradually reaches a thermodynamic equilibrium with a constant gas pressure. In this case, the calculated equilibrium gas pressure is around 48 bar.

7.2 Contact water mitigation

In this case, the mitigation effect of water directly in contact with the explosive is investigated. 100×100 particles are initially deployed exponentially (with the exponential factor 1.01) in the computational domain (one quarter of the geometry). Since more particles produce nearly the same results, the numerical results obtained by using 100×100 particles are regarded as the convergent solution. Different water shield thicknesses are examined. Figures 9 and 10 show the peak shock pressures and shock arrival times at the four observation points. The peak shock pres-

sure and shock arrival time are normalized by the corresponding peak shock pressure and shock arrival time without water mitigation at the same points, while the abscissa is the water shield thickness normalized by the initial explosive TNT thickness. As anticipated, the shock arrival time increases with enlarging the water shield thickness. It can be seen from Fig. 9 that putting water around explosive does lead to mitigation of peak shock pressures at all locations. The mitigation effect is stronger at nearer points and weaker at points further from the center. Varying the water shield thickness leads to different mitigation behavior. For a certain observation point, increasing the water shield thickness up to a certain value results in gradually decreasing peak shock pressures. The mitigation effect on the peak shock pressure reaches a maximum when the normalized water shield thickness approaches 1 (i.e. 0.025 m). Beyond this value, increasing the water shield thickness, on the contrary, leads to worse mitigation effect. In fact, since the density of water is much higher than that of air (approximately in 1000 times), when the explosive gas particles strike the water particles, the gas particles are suddenly slowed down with the rapid acceleration of the water particles due to momentum exchange. In the interaction process of the explosive gas and water particles, the water particles are compressed and heated. The momentum and energy exchange between the different particles mitigate the blast effect, and reduce peak shock pressures. On the other hand, the water shield, as a barricade and a mitigator of the shock, confines the outward burst of the gas particles. This confining effect actually raises peak shock pressures and acts as an offset to the mitigation effect. When increasing the water shield thickness, the momentum and energy exchange gradually slow down while the confining effect becomes stronger. Therefore, an optimum value of water shield thickness exists, on either side of which the mitigation effect is weaker. In other words, more water does not necessarily produce better mitigation effects. For the contact water mitigation case considered here, the normalized optimum water shield thickness is 1 (or 0.025 m without normalization), with the surrounding mitigation water weighing 1.84 times the TNT charge. This finding is of great importance for practical applications, and may provide a reference criterion for the design of water mitigation devices after taking into account the specifics of different situations.

Figures 11 and 12 show the density and pressure distributions at four instants for the calculated optimum water shield thickness. Similar to the above case of explosion in air, the initially square-shaped explosive gas and water particles gradually assume a circular shape. With the propagation of the shock, the water particles are compressed into a thinner layer. The pressures around the diagonals are higher than those at other positions of the same distance to the origin.

The final equilibrium gas pressure is determined by the thermodynamic equilibrium of the explosive gas, water and air in the confining chamber. The equilibrium gas pressures for different water shield thicknesses are listed in Table 4, normalized by the equilibrium gas pressure

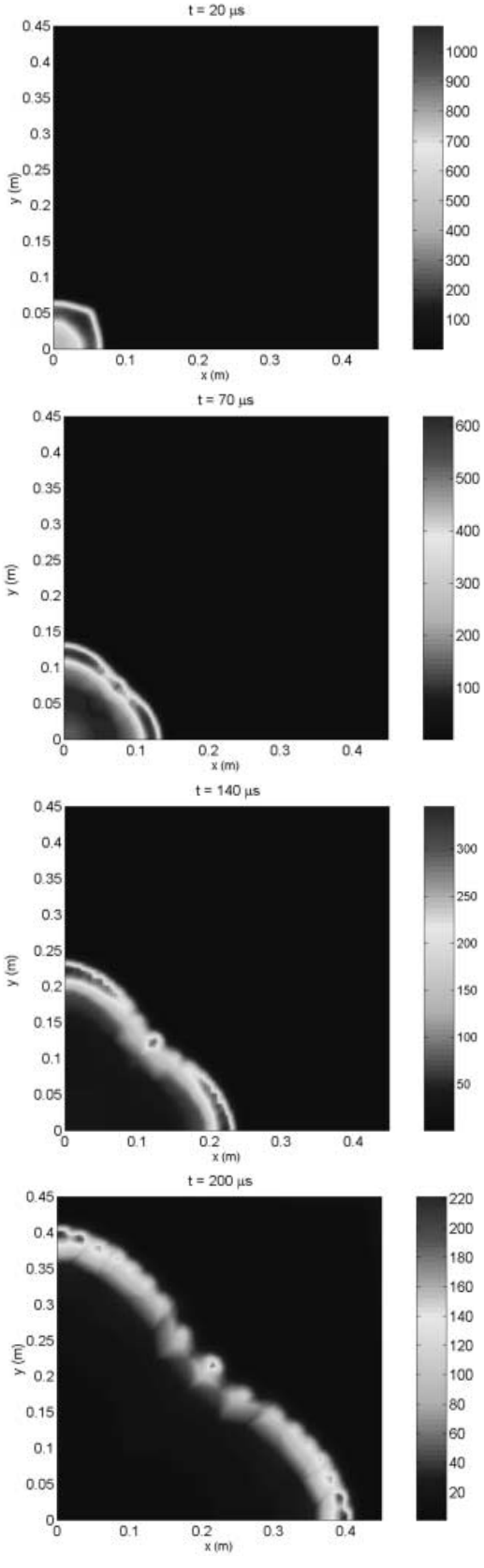

Fig. 11. Density evolution at t = 20, 70, 140, and 200 μs for the contact water mitigation with normalized water shield thickness 1

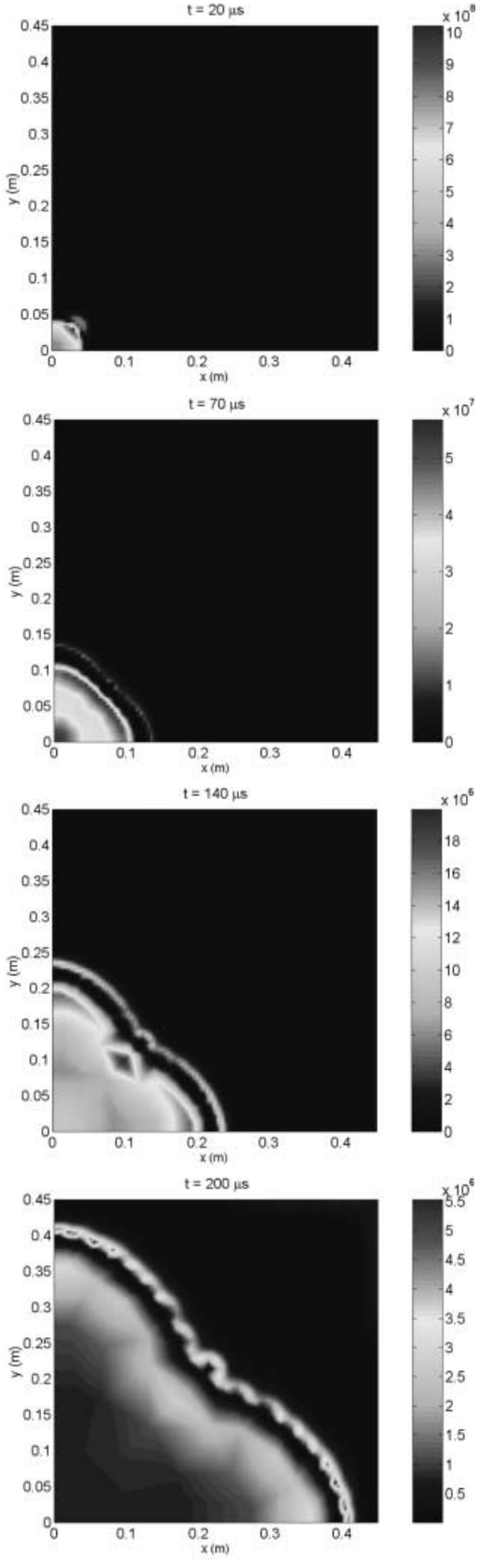

Fig. 12. Pressure evolution at t = 20, 70, 140, and 200 μs for the contact water mitigation with normalized water shield thickness 1

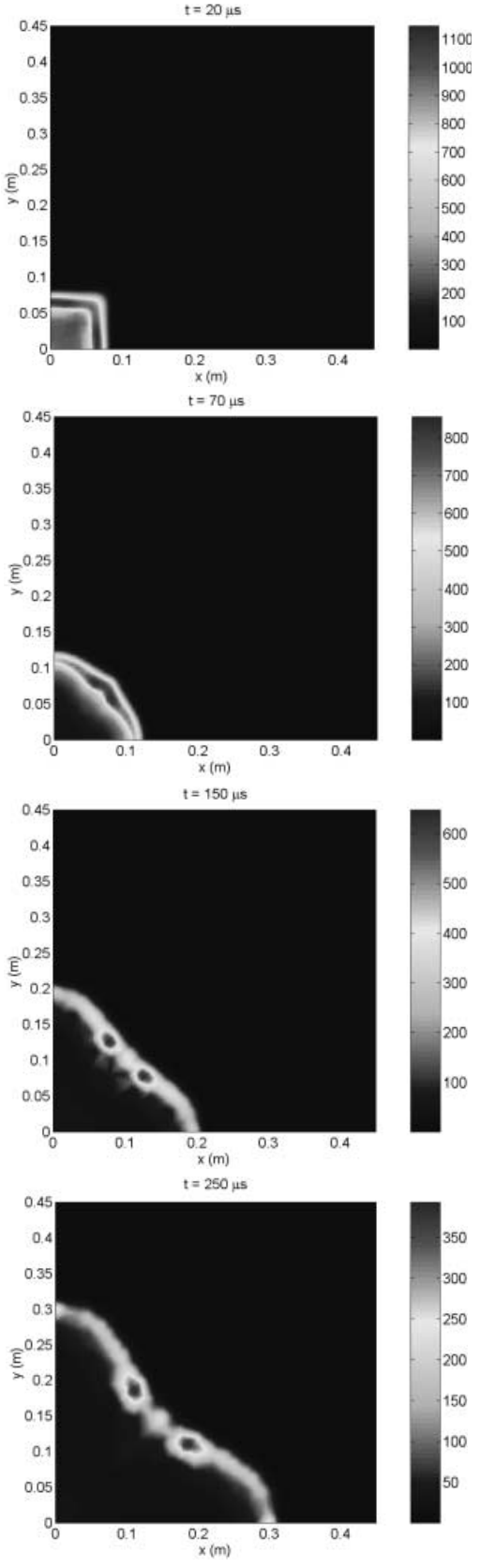

Fig. 13. Density evolution at t = 20, 70, 150, and 250 μs for the non-contact water mitigation with normalized air gap thickness 1 and water shield thickness 1

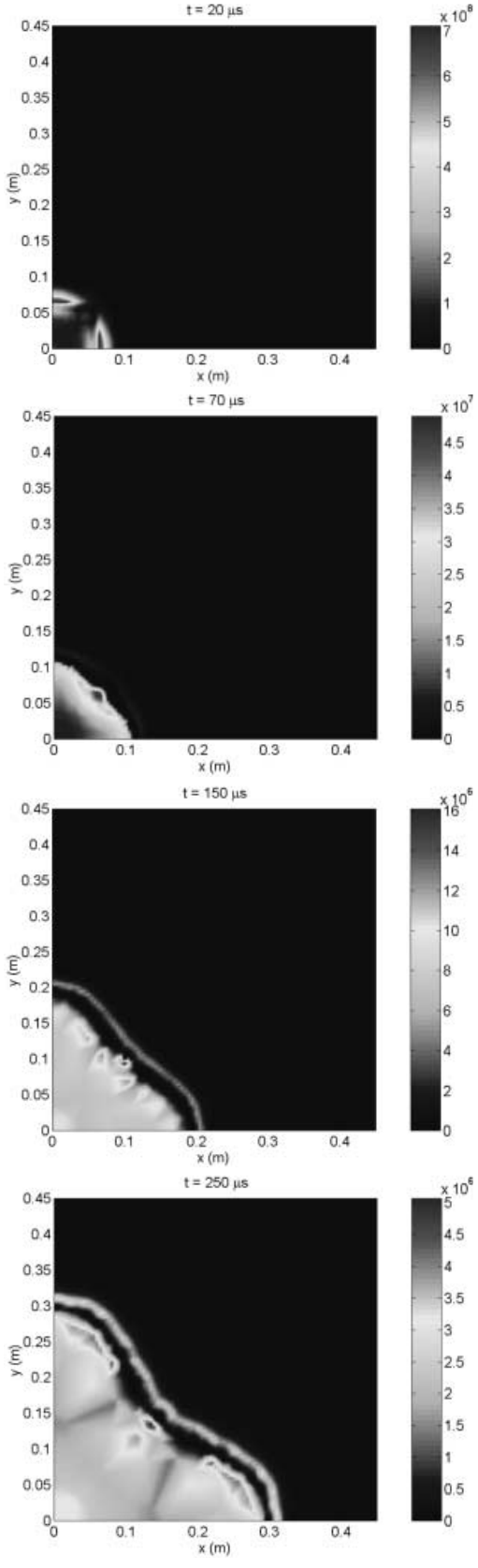

Fig. 14. Pressure evolution at t = 20, 70, 150, and 250 μs for the non-contact water mitigation with normalized air gap thickness 1 and water shield thickness 1

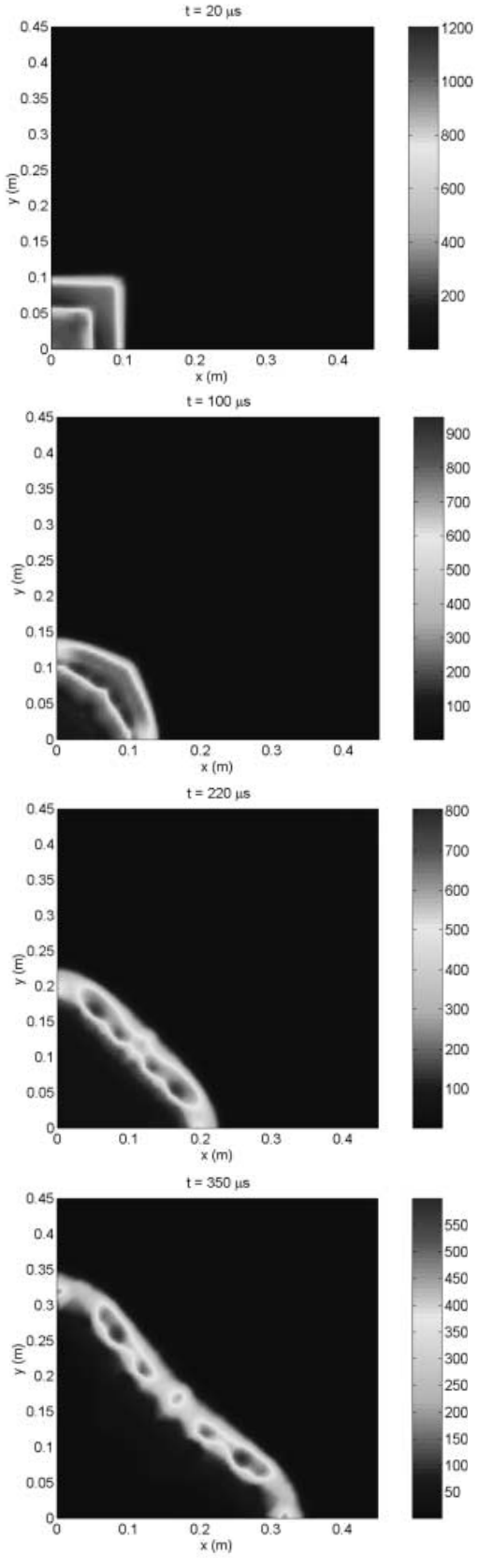

Fig. 15. Density evolution at t = 20, 100, 220, and 350 μs for the non-contact water mitigation with normalized air gap thickness 1 and water shield thickness 2

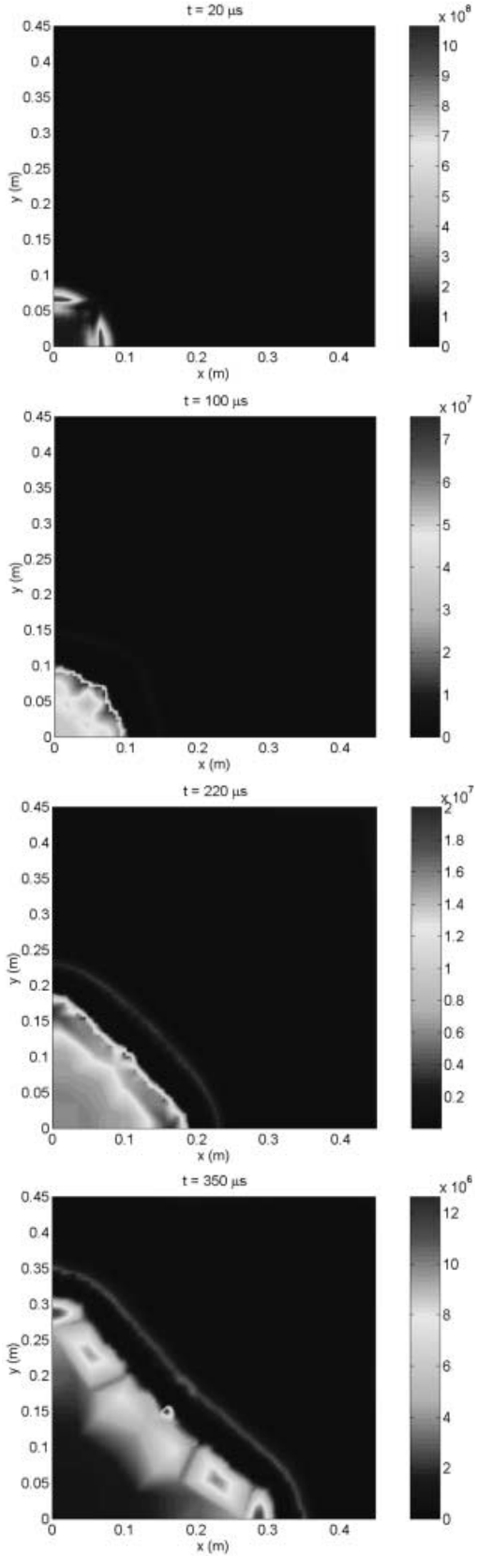

Fig. 16. Pressure evolution at t = 20, 100, 220, and 350 μs for the non-contact water mitigation with normalized air gap thickness 1 and water shield thickness 2

Table 4. Equilibrium gas pressures for the contact water mitigation

Water shield thickness	Equilibrium gas pressure (10^5 Pa)	Normalized gas pressure (%)
0	48.3	100
0.4	35.6	73.7
0.8	28.4	58.8
1.0	8.6	17.8
1.4	15.8	32.7
1.8	26.8	55.5

without water mitigation. The equilibrium gas pressure reduces for the given water shield thickness. The maximum reduction occurs when the normalized water shield thickness is 1, and the equilibrium gas pressure is around 17.8% of the equilibrium gas pressure of the explosion in air. This can also be explained from two points of view. Water absorbs and dissipates the released energy from the explosive gas when being compressed and heated. More water means better energy absorption effect and thus lower equilibrium gas pressure. On the other hand, more water occupies more space, which leads to higher equilibrium gas pressure. The influences from the two factors produce the optimum effect when an optimum water shield thickness is selected.

7.3 Non-contact water mitigation

When an air gap is placed between the explosive and water, the mitigation effect may be different from the above contact water mitigation case. The geometry of the air gap with respect to that of the water shield and the explosive charge may significantly change the peak shock pressure at a certain location as well as the final equilibrium gas pressure. In this study, an air gap with normalized thickness 1 (0.025 m) is employed with two different water shield thicknesses, 1 (0.025 m) and 2 (0.05 m). Figures 13 and 14 show the density and pressure evolution at the instants of 20, 70, 150 and 250 μs with water shield thickness 1. Comparing Fig. 13 with Fig. 11, and Fig. 14 with Fig. 12, it can be found that the shock arrival is obviously delayed. The peak shock pressures are further reduced, especially at locations nearer to the origin. The final equilibrium gas pressure is reduced to approximately 8 bar, that is about 16.6% of the equilibrium gas pressure without water mitigation. Figures 15 and 16 show the density and pressure evolution at the instants of 20, 100, 220 and 350 μs with water shield thickness increased to 2. Though the shock arrivals are further delayed, the peak shock pressures are higher than those in contact water mitigation. The calculated final equilibrium gas pressure is 11.4 bar, that is about 23.6% of the equilibrium gas pressure without water mitigation.

8 Conclusions

Water has been increasingly used to mitigate the blast effects from explosive detonations. In this paper, the meshless, Lagrangian method of smoothed particle hydrodynamics is applied to simulate water mitigation problems. The method is robust, computationally efficient, and easy to apply. Verification numerical tests of a one-dimensional TNT slab detonation and a spherical underwater explosion provide confidence when applying SPH to the simulation of water mitigation problems. Both contact and non-contact water mitigation are investigated with different water shield thicknesses. The simulation results, though obtained for small-scale simple cases and to be adjusted to different specific situations, are instructive for practical applications of water mitigation. From the numerical simulations and discussions, the following conclusions can be made:

- Putting a layer of water around explosive, either in direct contact or separated by an air gap, does mitigate the peak shock pressure as well as the final equilibrium gas pressure;
- For the contact water mitigation problem, there is an optimum water shield thickness for a given explosive charge. Around this optimum value, the best mitigation effect can be obtained; on either side of the optimum value, the mitigation effect becomes worse;
- For non-contact water mitigation, the relevant geometry of the explosive charge, air gap and water shield must be carefully investigated. A properly designed structure can produce even better mitigation effects as compared to contact water mitigation. Ill deployment of the water mitigation setup may result in poor, sometimes even reverse mitigation effect;
- Either for the contact or non-contact water mitigation, the mitigation effect on the equilibrium gas pressure is much more obvious than that on the peak shock pressure. In this study, the maximum reduction of the equilibrium gas pressure is up to 83.4%.

References

Chisum JE, Shin YS (1997) Explosion gas bubbles near simple boundaries. Shock Vib. 4(1):11–25

Chong WK, Lam KY, Yeo KS, Khoo BC, Liu GR, Chong OY (1998a) Computational study of water mitigation effects on an explosion inside a vented tunnel system. Explosive Safety, pp 118-124

Chong WK, Lam KY, Yeo KS, Khoo BC, Liu GR, Chong OY (1998b) Blast suppression using water in a tunnel system. In: Proceedings of the 3rd High Performance Computing Asia Conference, Singapore, vol 2, pp 968–982

Chong WK, Lam KY, Yeo KS, Liu GR, Chong OY (1999) A comparison of simulation's results with experiment on water mitigation of an explosion. Shock Vib. 6:73–80

Cole H (1948) Underwater explosions. Princeton University Press

Crepeau J, Needham C (1998) The effects of water on blast from the simultaneous detonation of 180 152 mm shells. 28th DDESB Seminar, Orlando, FL, USA

Dobratz BM (1981) LLNL Explosive Handbook. UCRL-52997, Lawrence Livermore National Laboratory, Livermore, CA

Forsen R, Carlberg A, Eriksson S (1996) Small scale tests on mitigation effects of water in a model of the KLOTZ Club Tunnel in Alvdalen. 27th DDESB Seminar, Las Vegas, NV, USA

Forsen R, Hansson H, Carlberg A (1997) Large scale test on mitigation effects of water in the KLOTZ Club installation in Alvdalen. FOA Report R-97-00470-311-SE, Defense Research Establishment, Sweden

Gingold RA, Monaghan JJ (1977) Smoothed particle hydrodynamics: theory and application to non-spherical stars. Mon. Not. Roy. Astron. Soc. 181:375–389

Hansson H, Forsen R (1997) Mitigation effects of water on ground shock: large scale testing in Alvdalen. FOA-R-97-311, Defense Research Establishment, Weapons and Protection Division, S-17290, Stockholm, Sweden

Keenan WA, Wager PC (1992) Mitigation of confined explosion effects by placing water in proximity of explosions. 25th DDESB Explosives Safety Seminar, Anaheim, CA, USA

Libersky LD, Petsheck AG (1993) High strain Lagrangian hydrodynamics – a three-dimensional SPH code for dynamic material response. J. Comput. Phys. 109:67–75

Liu MB, Liu GR, Zong Z, Lam KY (2000) Numerical simulation of underwater explosion by SPH. In: Atluri SN, Brust FW (eds) Advances in Computational Engineering and Science, pp 1475–1480

Liu GR, Liu MB, Lam KY, Zong Z (2001) Simulation of the explosive detonation process by using SPH methodology. In: Bathe KJ (ed) Computational fluids and solid mechanics. Elsevier Science Ltd., pp 323–326

Liu MB, Liu GR, Lam KY, Zong Z (2002) Computer simulation of the high explosive explosion using SPH methodology. Computers and Fluids (in press)

Lucy L (1977) A numerical approach to testing the fission hypothesis. Astron J. 82:1013–1024

Malvar LJ, Tancreto JE (1998) Analytical and test results for water mitigation of explosion effects. 28th DDESB Seminar, Orlando, FL, USA

Marchand KA, Oswald CJ, Plocyn MA (1996) Testing and analysis done in support of the development of a container for on-site weapon demilitarization. 27th DDESB Seminar, Las Vegas, NV, USA

Monaghan JJ (1992) Smoothed particle hydrodynamics. Annual Rev. Astron. Astrophys. 30:543–574

Monaghan JJ (1994) Simulating free surface flows with SPH. J. Comput. Phys. 110:399–406

Penney WG, Dasgupta HK (1942) British Report, RC 333

Randles PW, Libersky LD (1996) Smoothed particle hydrodynamics some recent improvements and applications. Comput. Methods Appl. Mech. Eng. 138:375–408

Shin YS, Chisum JE (1997) Modeling and simulation of underwater shock problems using a coupled Lagrangian-Eulerian analysis approach. Shock Vib. 4:1–10

Shin YS, Lee M, Lam KY, Yeo KS (1998) Modeling mitigation effects of water shield on shock waves. Shock Vib. 5:225–234

Steinberg DJ (1987) Spherical explosions and the equation of state of water. Report UCID-20974, Lawrence Livermore National Laboratory, Livermore, CA

Swegle JW, Attaway SW (1994) On the feasibility of using smoothed particle hydrodynamics for underwater explosion calculations. Comput. Mech. 17:151–168

Zhang SZ (1976) Detonation and its applications. Press of National Defense Industry, Beijing

Zhao HZ, Lam KY, Yeo KS, Khoo BC, Liu GR (1998) Water mitigation effects on the detonation in a confined chamber. In: Proceedings of the 3rd High Performance Computing Asia Conference, Singapore, vol 1, pp 808–811

Zhao HZ (2001) Water effects on shock wave delay in free fields. Explosion and Shock Waves (in Chinese) 21(1):26–28